energies

MDPI

Article

The Eddy Dissipation Concept—Analysis of Different Fine Structure Treatments for Classical Combustion

Markus Bösenhofer [1,2,*,†], Eva-Maria Wartha [1], Christian Jordan [1] and Michael Harasek [1]

1 Institute of Chemical, Environmental & Bioscience Engineering, Technische Universität Wien, Getreidemarkt 9/166, 1060 Vienna, Austria; eva-maria.wartha@tuwien.ac.at (E.-M.W.); christian.jordan@tuwien.ac.at (C.J.); michael.harasek@tuwien.ac.at (M.H.)

2 K1-MET GmbH, Stahlstraße 14, 4020 Linz, Austria

* Correspondence: markus.boesenhofer@tuwien.ac.at; Tel.: +43-1-58801-166251

† Current address: Institute of Chemical, Environmental & Bioscience Engineering, Technische Universität Wien, Getreidemarkt 9/166, 1060 Vienna, Austria.

Received: 12 June 2018; Accepted: 19 July 2018; Published: 20 July 2018

Abstract: The Eddy Dissipation Concept (EDC) is common in modeling turbulent combustion. Several model improvements have been proposed in literature; recent modifications aim to extend its validity to Moderate or Intense Low oxygen Dilution (MILD) conditions. In general, the EDC divides a fluid into a reacting and a non-reacting part. The reacting part is modeled as perfectly stirred reactor (PSR) or plug flow reactor (PFR). EDC theory suggests PSR treatment, while PFR treatment provides numerical advantages. Literature lacks a thorough evaluation of the consequences of employing the PFR fine structure treatment. Therefore, these consequences were evaluated by employing tests to isolate the effects of the EDC variations and fine structure treatment and by conducting a Sandia Flame D modeling study. Species concentration as well as EDC species consumption/production rates were evaluated. The isolated tests revealed an influence of the EDC improvements on the EDC rates, which is prominent at low shares of the reacting fluid. In contrast, PSR and PFR differences increase at large fine fraction shares. The modeling study revealed significant differences in the EDC rates of intermediate species. Summarizing, the PFR fine structure treatment might be chosen for schematic investigations, but for detailed investigations a careful evaluation is necessary.

Keywords: Eddy Dissipation Concept (EDC); turbulent combustion; plug flow reactor (PFR); perfectly stirred reactor (PSR); reactive flow modeling; Sandia Flame D; OpenFOAM®; computational fluid dynamics (CFD); fine structure treatment/closure

1. Introduction

Nowadays, the Eddy Dissipation Concept (EDC) [1–3] is very common in turbulent combustion modeling. Since the initial publication of the EDC in the 1970s, several modifications of the EDC were proposed in literature [4–8], all of them claiming to improve the modeling results. In recent years, emphasis is on the extension of the EDC for Moderate or Intense Low oxygen Dilution (MILD) combustion conditions [7–9]. In contrast to classical turbulent combustion, MILD combustion features widely distributed reaction zones and slower reactions due to lower oxygen concentrations as well as slightly lower turbulence [10–13]. In classical turbulent combustion, chemical reactions occur only in small areas, the so-called fine structures, where educts are mixed at molecular scale. These fine structures are of Kolmogorov length scale in at least two spatial dimensions and of larger scale in the third [3,4,14,15]. A fine structure share (γ^*) and a fine structure residence time (τ^*) are defined for characterization based on turbulence parameters. The non-reacting fluid is called the surroundings in the EDC context. At sufficiently high Reynolds numbers, combustion reactions are limited by the

mixing rate only, and an infinitely fast chemistry assumption is possible. However, if turbulence and turbulent mixing decrease, the reaction progress can be limited by either mixing or chemistry. In this regime, finite rate chemistry is necessary to accurately describe the turbulence-chemistry interaction [7,12,13]. When using detailed chemistry with the EDC, the fine structures are typically treated as perfectly stirred reactors (PSRs), since educts are mixed on a molecular scale and mass is exchanged with the surroundings [4]. The fine structure state is determined by solving the PSR to steady-state, which is numerically expensive due to the strong nonlinearity in the reaction source terms. Some EDC implementations, therefore, treat the fine structures as plug flow reactors (PFR) [7,16–19]. These PFRs are solved for the fine structure residence time, implying that the fine structures are spatially isolated structures in the fluid only evolving in time. Since fine structure residence times are typically small (approx. $\mathcal{O}\left(10^{-7}\right)$ to $\mathcal{O}\left(10^{-3}\right)$ seconds) for classical turbulent combustion, the numerical effort to solve the detailed chemistry in a PFR is significantly reduced. However, the latter approach is not in line with the EDC theory. Although the PFR fine structure treatment was employed in many published research works, e.g., [16–21], only De et al. [17], Li et al. [16], and Lewandowski and Ertesvaag [18] commented on the consequences of the PFR simplification. However, none of them performed an in-depth analysis of species profiles and species consumption rates.

De et al. [17] state that the PSR and PFR results are only similar for slow reactions having little heat tone. However, they did not provide any evidence for this. Only recently, Li et al. [16] published a numerical study of the Adelaide Jet in Hot Co-flow (JHC) flame. Besides other investigations, they compared species concentration and temperature profiles obtained by PSR and PFR fine structure treatment. The presented data indicates good agreement between main species and temperature, while concentrations for minor or intermediate species differ slightly. Therefore, they conclude that the PFR approach could be used instead of the PSR approach without loss of accuracy. An in-depth analysis of the results is missing. Lewandowski and Ertesvåg [18] concluded that the PSR and PFR approaches should give comparable results, since the steady-state solution of the PSR equations is of a similar form to the PFR solution. However, no numerical data to prove this conclusion was shown. In contrast to previous works, this work focuses on an in-depth analysis of the consequences of the PFR simplification and is meant to shed additional light on the comparisons available in literature. The results presented by Li et al. [16] indicate discrepancies in the minor species concentration under MILD combustion conditions. Since reactions are more intense (faster and higher heat release) in classical combustion than in MILD combustion, the differences between PSR and PFR results are expected to increase for classical combustion, e.g., Sandia Flame D [22,23]. Moreover, no data on species consumption/production rates have been published in literature so far. However, these rates reveal more details about the combustion process. This work aims to extend the knowledge on the different aspects of the EDC, e.g., model improvements and fine structure treatment, and for the first time gives a thorough comparison of the PSR and PFR results. For this purpose, first the EDC and its modifications are discussed, followed by an evaluation of the model differences. Furthermore, the PSR and PFR fine structure treatments are tested on a simple case. Eventually, the findings of the preliminary tests are challenged with a Sandia Flame D [22,23] modeling study. The study is conducted with a custom EDC extension for OpenFOAM® [24].

2. Theory

The EDC splits the reacting fluid into a reacting zone (fine structures) and a non-reacting zone (surroundings). The fine structures are of vortex-sheet or tubelike shape and their size is of Kolmogorov scale in two dimensions but at bigger scale in the third dimension [3,4,14,15]. Reactions occur in those spatially isolated regions, where educt gas phase species mix at the molecular scale. This is done by turbulent mixing in the Kolmogorov structures where fluid motion is dissipated to thermal energy due to viscous forces. Ertesvåg and Magnussen [25] compared the EDC theoretical turbulence energy cascade presumed for the EDC with turbulence energy spectra of reacting flows and showed that cascade reproduces the energy spectrum well. The different EDC modifications are discussed in more

detail in the next paragraphs. There, the fine structure, surrounding and fluid mean properties are denoted with *, $^\circ$ and $^-$, respectively.

2.1. 'EDC1981'

In the original EDC [3], the fine structure reaction rate R_i^* is equal to a mass transfer rate between the fine structures and the surroundings and is calculated as follows for species i:

$$R_i^* = \frac{\rho^*}{\tau^*}\left(\frac{c_i^\circ}{\rho^\circ} - \frac{c_i^*}{\rho^*}\right). \tag{1}$$

τ^* is the fine structure residence time or EDC mixing time, ρ^* and ρ° are the fine structure and surroundings densities, and c_i^* and c_i° are the fine structure and surrounding concentrations of species i. The inverse fine structure residence time is proportional to the dimensionless fine structure mass transfer rate ($\dot{m}^*$). The fine structure and surrounding quantities are linked by the fluid average properties and the fine structure mass share γ^*:

$$\overline{\Psi} = \Psi^\circ\left(1-\gamma^*\right) + \Psi^*\gamma^*. \tag{2}$$

A dimensionless fine structure length fraction is defined as the cubic root of the fine structure share:

$$\gamma_L = \sqrt[3]{\gamma^*}. \tag{3}$$

The fine structure length fraction γ_L and the fine structure residence time τ^* are calculated as ratios of the turbulent kinetic energy (k), the turbulent dissipation rate (ϵ), and the model constants C_τ or C_γ. An alternative definition based on the turbulent Reynolds number (Re_t, see Equation (4)) is also possible. The model constants are proportional to the C_{D1} and C_{D2} constants of the turbulent energy cascade [25]:

$$Re_t = \frac{k^2}{\epsilon\nu}, \tag{4}$$

$$\gamma_L = \left(\frac{3C_{D2}}{4C_{D1}^2}\right)^{\frac{1}{4}}\left(\frac{\nu\epsilon}{k^2}\right)^{\frac{1}{4}} = C_\gamma\left(\frac{\nu\epsilon}{k^2}\right)^{\frac{1}{4}} = C_\gamma Re_t^{-1/4}, \tag{5}$$

$$\tau^* = \left(\frac{C_{D2}}{3}\right)^{\frac{1}{2}}\left(\frac{\epsilon}{\nu}\right)^{\frac{1}{2}} = C_\tau\left(\frac{\epsilon}{\nu}\right)^{\frac{1}{2}} = C_\tau Re_t^{-1/2}\frac{k}{\epsilon}. \tag{6}$$

By substituting Equations (3) and (2) into Equation (1) and replacing the fine structure mass transfer rate with the mean mass transfer rate ($\dot{m} = \dot{m}^*\gamma_L^3 = \gamma_L^3/\tau^*$), the mean reaction rate is obtained as:

$$\overline{R}_i = \frac{\overline{\rho}}{\tau^*}\frac{\gamma_L^3\chi}{1-\gamma_L^3\chi}\left(\overline{Y}_i - Y_i^*\right). \tag{7}$$

$\overline{\rho}$, $\overline{Y_i}$, and Y^* denote the mean density, and the mean and the fine structure mass fractions of species i. χ represents the reacting fraction of the fine structures. and is assumed to be unity, although this might be wrong, especially for low turbulent flows as indicated by Lewandowski et al. [26]. They also speculate a relation of χ and Re_t at least for MILD combustion conditions [26,27].

If the reacting parts of the fine structures are assumed to be homogeneously mixed, they can be modeled as perfectly stirred reactors (PSR) [4]. The PSR has to be solved to steady-state in order to obtain the fine structure composition and, thus, the EDC reaction rates. Since computing the steady-state is numerically expensive, the fine structures are alternatively treated as plug flow reactors (PFR) and solved for the fine structure residence time [17].

2.2. 'EDC1996'

In 1996, Gran and Magnussen [5] proposed modifying the mean reaction rate to include mixing effects of fresh gas and fine structures. The conversion ratio of the mass exchange rate is changed from γ_L^3/τ^* to γ_L^2/τ^*. Accordingly, the mean reaction rate changes to:

$$\overline{R}_i = \frac{\overline{\rho}}{\tau^*} \frac{\gamma_L^2 \chi}{1 - \gamma_L^3 \chi} \left(\overline{Y}_i - Y_i^* \right). \tag{8}$$

2.3. 'EDC2005'

In 2005, Magnussen [6] proposed a modification of the fine structure definition ($\gamma^{*'}$) to incorporate the fact that reactions can extend outside the fine structures (Equation 10). Therefore, the mean reaction rate is modified to:

$$\overline{R}_i = \frac{\overline{\rho}}{\tau^*} \frac{\gamma_L^2 \chi}{1 - \gamma_L^2 \chi} \left(\overline{Y}_i - Y_i^* \right), \tag{9}$$

$$\gamma^{*'} = C_\gamma^{\frac{1}{2}} \left(\frac{\nu \epsilon}{k^2} \right)^{\frac{1}{2}} = \gamma_L^2. \tag{10}$$

Moreover, the relation between the mean fluid properties and the surrounding and fine structures changes:

$$\overline{\Psi} = \Psi^\circ \left(1 - \gamma^{*'} \right) + \Psi^* \gamma^{*'}. \tag{11}$$

2.4. 'EDC2016'

Recently, emphasis is put on the applicability of the EDC to non-classical combustion conditions, e.g., MILD combustion. First approaches tried to modify the EDC model constants to improve results [9,17,20,21]. However, these modifications were only applicable for specific cases. Parente et al. [7] proposed a more sophisticated approach to adapt the EDC. Since Kolmogorov eddies enter and thicken the reaction zone, the characteristic fine structure velocity is proportional to the flame speed in MILD combustion [12]. Therefore, the turbulent energy cascade is related to the Damköhler number at Kolmogorov scale (Da_η) and the turbulent Reynolds number (Re_t). The modified energy cascade gives alternative definitions of the model constants C_γ and C_τ, which can be seen as local qualitative estimates:

$$C_\gamma = \frac{3C_{D2}}{4C_{D1}^2}^{\frac{1}{4}} \propto \sqrt{(Re_T + 1)\, Da_\eta}, \tag{12}$$

$$C_\tau = \frac{C_{D2}}{3}^{\frac{1}{2}} \propto \frac{1}{Da_\eta \sqrt{Re_T + 1}}. \tag{13}$$

The mean reaction rate is calculated according to Equation (8) by changing the model constants when calculating γ_L Equation (5) and τ^* Equation (6). Both EDC model constants are limited to their default values, e.g., C_γ below 2.1377 and C_τ above 0.4082.

2.5. 'EDC2017'

Bao [8] modified Parente's idea and eliminated the flame speed from the derivations of the model constants by substituting it with the characteristic length and the chemical time scale $S_L = L^*/\tau_c^* \propto \sqrt{\frac{\nu}{\tau_C}}$. Since the unknown proportional factor in the flame speed definition is eliminated, a quantitative relation for the local model constants C_τ and C_γ was derived. The definitions of Bao and Parente et al. show similar structures:

$$C_\gamma = \left(\frac{3C_{D2}}{4C_{D1}^2} \right)^{\frac{1}{4}} = \sqrt{\frac{3}{2}\,(Re_T + 1)} Da_\eta^{\frac{3}{4}}, \tag{14}$$

$$C_\tau = \left(\frac{C_{D2}}{3}\right)^{\frac{1}{2}} = \frac{1}{2}\frac{1}{Da_\eta\sqrt{Re_T+1}}. \tag{15}$$

The procedure for calculating the mean EDC rate is taken from Parente et al.

The review of the different EDC modifications shows three approaches for the model adaption: conversion from fine structure to mean reaction rates [5,6], modified model constants, e.g., static [17,20,21] or dynamic based on local properties [7,8], and fine structure treatment [5,16,17]. Figure 1 summarizes the differences of the EDC modifications available in literature based on a schematic illustration of a representative fine structure. The arrows surrounding the fine structures indicate the relative intensity of the mass transfer between non-reacting surroundings and the fine structures, which differs between the EDC versions. In case of the EDC-MILD, the colored arrows shall indicate that the fine fraction share and mass transfer rates can vary.

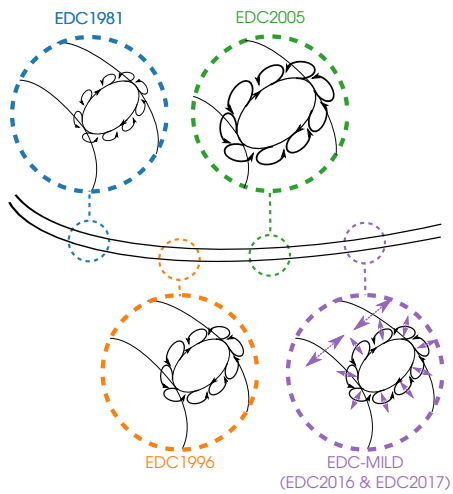

Figure 1. Schematic view of the different Eddy Dissipation Concept (EDC) modifications available in literature. indicates the fine structures, while represents the mass transfer between them and the surroundings. illustrates the variable fine structure fractions and mass transfer intensities occurring in the EDC modifications for Moderate or Intense Low oxygen Dilution (MILD) combustion. Symbol sizes indicate their relative relations.

3. The Mean Reaction Rate Expression

Converting fine structure reaction rates to fluid mean rates by a characteristic volumetric ratio would be a logical choice Equation (16). However, different conversion ratios based on adapted model assumptions have been proposed in literature. Gran and Magnussen [5] modified the conversion of the mass transfer rate to $\dot{m} = \dot{m}^*\gamma_L^2$ Equation (17). Actually, this means reaction rates are converted by a characteristic surface to volume ratio instead of a characteristic volume ratio. Keeping in mind that γ_L should be between 0 and 1 to satisfy $\gamma^* \leq 1$, it is obvious that this modification increases the average reaction rate compared to the characteristic volume ratio conversion. In 2005, Magnussen [6] proposed a new modification Equation (18) based on a characteristic surface ratio. Therefore, both the mass transfer rate and the surrounding species mass fraction are converted by γ_L^2 and $1-\gamma_L^2$, respectively. This surface ratio conversion gives the highest average reaction rates. In general, the conversion expressions differ only by the exponents of the characteristic fine structure length fraction γ_L in the numerator and denominator. The following equations summarize the conversion factors of the EDC1981, EDC1996 and EDC2005 modification:

$$EDC1981: \frac{\gamma_L^3}{1-\gamma_L^3}, \tag{16}$$

$$EDC1996: \frac{\gamma_L^2}{1-\gamma_L^3}, \tag{17}$$

$$EDC2005: \frac{\gamma_L^2}{1-\gamma_L^2}. \tag{18}$$

Obviously, all three expressions have a singularity near $\gamma_L = 1$. Moreover, they can be approximated by γ_L^2 or γ_L^3 if $\gamma_L << 1$, respectively. However, since the fine structure residence time (τ^*) should be smaller than or equal to a characteristic mixing time (τ_{mix}), the fine structure fraction should be limited in order to ensure a ratio (R_τ) of the fine structure to the mixing time below unity, e.g., for the original EDC [16–18,28]:

$$R_\tau = \frac{\tau^*}{\tau_{mix}} = \frac{\gamma_L^3}{1-\gamma_L^3} < 1. \tag{19}$$

As a result, the maximum γ_L is different for the three conversion ratios and has values between 0.70 and 0.79. In contrast, Lewandowski et al. [26] proposed the trivial condition based on the mean and fine structure reaction rates, which give $\tau_{mix} = \tau^*/\gamma_L^3$:

$$R_{timescale} = \frac{\tau^*}{\tau_{mix}} = \frac{\tau^*\gamma_L^3}{\tau^*} < 1. \tag{20}$$

Requiring $\gamma_L < 1$ allows significant higher species reaction rates. According to Lewandowski et al., a limitation of the fine structure length fraction is only necessary if the employed mixing time scale deviates from the EDC mixing time scale. Figure 2 shows the influence of the different conversion ratios on the average reaction rate. The top diagram depicts the conversion factor for all three conversion ratios, the dashed line represents the maximum conversion ratio to obey Equation (19). The bottom diagram depicts the conversion factors normalized by the volume ratio conversion factor Equation (7) over the whole γ_L range. Both the surface to volume and the surface ratio give similar values for $\gamma_L < 0.4$. Starting at $\gamma_L = 0.4$, the surface to volume ratio approaches the volume conversion ratio.

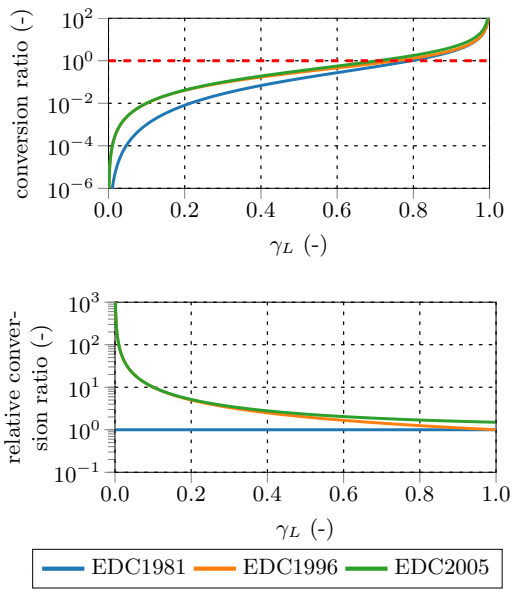

Figure 2. Comparison of the proposed EDC reaction rate conversion factors; dashed line represents limit according to Equation (19).

The normalized conversion ratios reveal that the surface conversion ratio results in approximately 1.5 times higher reaction source terms than the volume conversion ratio at high γ_L. In contrast, at low γ_L values (especially if smaller than 0.1), the surface to volume and the surface conversion ratios give several times higher reaction rates than the volume conversion ratio. The surface to volume conversion ratio is a hybrid version of the other two ratios: it is similar to the surface conversion ratio for low and similar to the volume conversion ratio for high γ_L values. In general, the relative differences arising due to the different conversion ratios are higher at low γ_L values (exceeding a factor of 100) and reduce to a factor below 2 for $\gamma_L > 0.5$. However, the absolute differences are small for low γ_L, since the conversion ratios are small compared to unity ($\gamma_L << 1$).

4. Model Constant Modification

The C_γ and C_τ EDC constants were adapted to reproduce MILD combustion conditions by Parente et al. [7] and Bao [8]. The Damköhler number at Kolmogorov scale (Da_η) is of order unity in this combustion regime. Thus, the influence of the different model formulations is investigated for $Da_\eta < 2$ and turbulent Reynolds numbers (Re_t) up to 1000. Figure 3 shows γ_L (top) and τ^* (bottom) for the modified EDC constants normalized by the results for the standard EDC constants on a double-log plot. The fine structure length fraction (γ_L) increases with increasing Damköhler number at a given Kolmogorov scale (Da_η) and increasing turbulent Reynolds number (Re_t). EDC2016 and EDC2017 modifications reach the original fine structure length fraction below a Damköhler number of around unity. If C_γ is clipped by the EDC1981 value, the modifications affect the results for slow reactions in less turbulent regions. The slope of EDC2016 is higher, but the intercept is significantly lower than for the EDC2017.

The fine structure residence time (τ^*) behaves opposite to the fine structure length fraction. The EDC2016 and EDC2017 residence times approach the EDC1981 values between Damköhler numbers of 0.1 and 1 for the investigated turbulent Reynolds numbers (Re_t). The slopes of the EDC2016 and EDC2017 modifications are identical in the double-log representation, but the intercepts of the EDC2016 are significantly lower, indicating smaller fine structure residence times.

Farokh and Birouk [20,21] showed that the influences of C_τ and C_γ on temperature and species concentrations depend on the turbulence level. They performed a modeling study on Sandia Flames A and B; Flame A is a low turbulent flame ($\mathrm{Re}_{jet} \approx 1100$), while Flame B is more turbulent ($\mathrm{Re}_{jet} \approx 17500$). In case of low turbulence, the time scale ratio according to Equation (19) would exceed unity and, thus, fine structure shares are limited to ensure a proper ratio between mixing and fine structure residence time. If C_τ is decreased in these regions, reaction rates increase and vice versa. In contrast, if the critical Reynolds number is exceeded, an increase of C_τ gives higher reaction rates. For highly turbulent flames, e.g., Flame B, higher C_γ values result in higher temperatures and reaction rates. The influence of C_τ is less distinct than the one of C_γ. However, increased C_τ constants gave lower temperatures before and after the temperature peak, while the peak temperature was virtually the same. At peak temperatures, reactions are mixing controlled, since chemistry time scales are fast there. Up- and downstream, temperatures decrease and reactions become either mixing or chemical controlled.

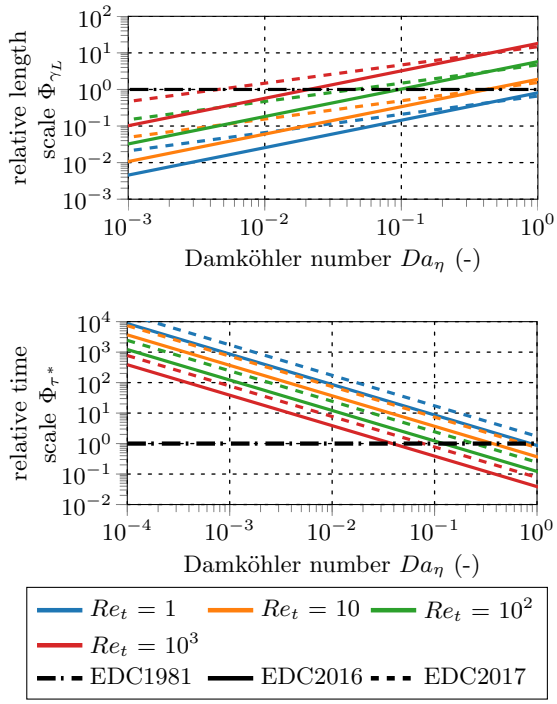

Figure 3. Comparison of the fine structure share (**top**) and the fine structure residence time (**bottom**) as functions of the Damköhler number at Kolmogorov scale (Da_η) and turbulent Reynolds number (Re_t) of the EDC2016 and EDC2017 normalized by the results using the EDC1981.

5. Fine Structure Treatment—Perfectly Stirred Reactor (PSR) vs. Plug Flow Reactor (PFR)

According to Magnussen [4], fine structures can be seen as perfectly stirred reactors (PSR), since they provide a perfect analogy: the fine structure residence time τ^* corresponds to the PSR residence time. The PSR inlet concentrations are equal to the species concentrations of the non-reacting surroundings and the PSR outlet concentrations are the fine structure concentrations. Neglecting radiative or diffusive thermal losses of the fine structures, the PSR is described by the following set of equations for species mass fraction (Y_i), enthalpy (h), and pressure (p):

$$\frac{dY_i}{dt} = \dot{\omega}_i^* + \frac{1}{\tau^*}\left(Y_i^\circ - Y_i^*\right), \tag{21}$$

$$\frac{dh}{dt} = 0, \tag{22}$$

$$\frac{dp}{dt} = 0. \tag{23}$$

$\dot{\omega}_i^*$ is the chemical species reaction rate, while the second term on the right hand side (RHS) represents the mixing between fine structures and surroundings. The PSR is solved to steady-state to obtain the fine structure composition. Solving this set of ordinary differential equations (ODE) is numerically expensive, since the chemical source terms are highly nonlinear. Furthermore, under certain conditions, periodic oscillating states might occur in PSRs, although steady input parameters are employed, due to chemical kinetic effects. An example of such a periodic oscillating state is given in Figure 4. A stoichiometric hydrogen mixture at 800 K and 0.1 bar is combusted in a PSR with a residence time of 0.75 s employing the kinetic mechanism of Connaire et al. [29]. The open source tool Cantera [30] was employed for the PSR calculation. Moreover, Cantera tutorials inspired the authors for the periodic oscillation example.

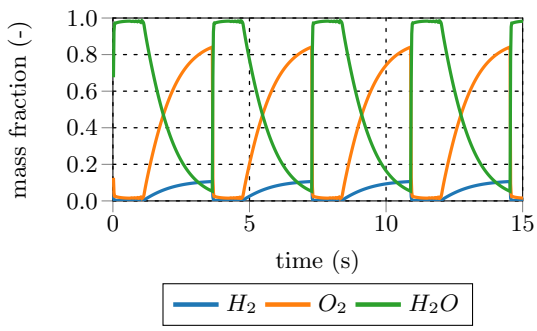

Figure 4. Example oscillating behavior for hydrogen combustion in a perfectly stirred reactor (PSR).

A convenient way to get rid of the instabilities and to reduce the numerical effort, is to neglect the mixing term between the fine structures and the surroundings [9,16–18]. This approach is referred to as the plug flow reactor (PFR) approach, since back-mixing is ignored in the species conservation equations and only chemistry is integrated over time. The integration time reduces to the fine structure residence time (τ^*). Using the same assumptions as for the PSR, the PFR is described by the following set of equations:

$$\frac{dY_i}{dt} = \dot{\omega}^*, \tag{24}$$

$$\frac{dh}{dt} = 0, \tag{25}$$

$$\frac{dp}{dt} = 0. \tag{26}$$

Obviously, the results of these two reactor types should differ when using the same starting values. Since the fine structure species concentrations directly influence the mean reaction rates, the results using the PSR and PFR approach in flame modeling are expected to differ. Figure 5 gives a conceptional illustration of the PSR and the PFR fine structure treatment. In case of the PSR treatment, small eddies forming at the surface or diffusion effects enable mass exchange with the surroundings. This is indicated by tiny eddies surrounding the fine structures. In contrast, the PFR approach assumes isolated, possibly smooth structures lacking mass transfer with the surroundings. Treating the fine structures as PFR should increase the EDC mean rates compared to the PSR approach for fast reactions, since no educts are back-mixed to the PFR.

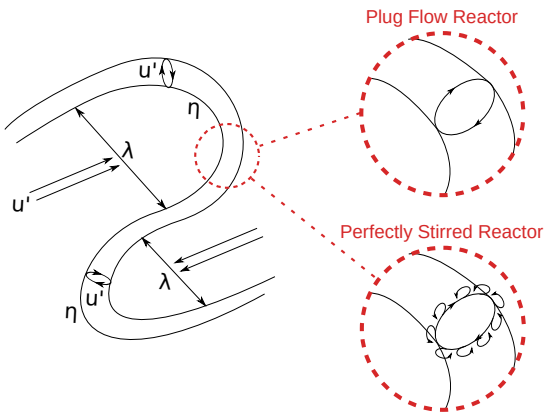

Figure 5. Schematic view of the different fine structure treatments, adapted from [31]. indicates the fine structures, while indicates the mass transfer between them and the surroundings.

For a better illustration, a case study for different γ^* and τ^* values was conducted. A simple test case representing a single fluid element was used. The employed chemical mechanism for all calculations was the GRI3.0, which is an optimized methane combustion mechanism [32]. In order to

investigate the influence of the reactor type, the ratio of the PFR and PSR mean reaction rate is taken. If the initial values are identical, the ratio reduces to the ratio of the difference between the mean and fine structure mass fractions:

$$\Phi_R = \frac{\overline{R}_{i,PFR}}{\overline{R}_{i,PSR}} = \frac{\overline{Y}_{i,PFR} - Y^*_{i,PFR}}{\overline{Y}_{i,PSR} - Y^*_{i,PSR}}. \tag{27}$$

This ratio is investigated for the main combustion educts and products (CH_4, CO, CO_2, H_2, H_2O, O_2) and the main combustion radical species (H, O, OH) to quantify the effect of the fine structure treatment on the mean reaction rate.

Three sets of initial mole fractions were employed for the simple test case: lean and stoichiometric mixtures of main species, and a high radical mixture representing the reaction zone of a methane flame. Initial temperatures were set to 1000 K, and 2000 K for the main species and to 2000 K, and 2200 K for the high radical mixture, respectively. The fine structure residence times were chosen rather arbitrarily, but should reflect typical residence times. A PSR model based on Cantera [30] was employed for the test cases. Tables 1 and 2 summarize the initial conditions of the main species and radical species test cases, respectively.

Table 1. Initial values for the simple perfectly stirred reactor (PSR) versus plug flow reactor (PFR) fine structure treatment main species test case.

	Stoichiometric	**Lean**
γ^* (-)	0.1–0.6	0.1–0.6
τ^* (s)	1–10^{-3}	1–10^{-3}
temperature (K)	1000 and 2000	1000 and 2000
CH_4 ($\frac{mol}{mol}$)	0.10	0.05
N_2 ($\frac{mol}{mol}$)	0.70	0.725
O_2 ($\frac{mol}{mol}$)	0.20	0.225

Table 2. Initial values for the simple PSR versus PFR fine structure treatment radical species test case.

	Radical
γ^* (-)	0.1–0.6
τ^* (s)	1–10^{-7}
temperature (K)	2000 and 2200
C_2H_2 ($\frac{mol}{mol}$)	0.000191
CH_4 ($\frac{mol}{mol}$)	0.000501
CO ($\frac{mol}{mol}$)	0.0209
CO_2 ($\frac{mol}{mol}$)	0.103
H ($\frac{mol}{mol}$)	0.000112
H_2 ($\frac{mol}{mol}$)	0.000802
H_2O ($\frac{mol}{mol}$)	0.105
N_2 ($\frac{mol}{mol}$)	0.724
NO ($\frac{mol}{mol}$)	0.000236
O ($\frac{mol}{mol}$)	0.00102
O_2 ($\frac{mol}{mol}$)	0.0412
OH ($\frac{mol}{mol}$)	0.0034

Figures 6 and 7 show representative results of the total 192 data sets. In general, the differences in the mean reaction rates increase at bigger fine structure scales (γ^*), while they decrease for longer fine structure residence times (τ^*). For $\gamma^* = 0.1$, mean reaction rates of most species are in the same range. In other words, PSR and PFR approaches give similar results for the mean rates in the case

of small fine structure length fractions. Since classical turbulent combustion occurs in small isolated structures [3,12,13], both fine fraction treatments should give similar results. In contrast, in case of MILD combustion, reactions occur in a significant portion of the fluid and, therefore, the PFR approach will give different EDC reaction rates than the PSR approach.

Comparing the main and radical test case results reveals that the differences in the mean reaction rates are in general higher for the radical species cases. This is caused by the pronounced radical pool and the resulting small characteristic chemical time scales. The results confirm the findings of De et al. [17] that both approaches give similar results only for slow and slightly exothermic reactions. The differences in the reaction rates between the PSR and PFR fine structure treatment depend on the fine structure properties (γ_L, τ^*), the fine structure state (temperature, pressure, chemical composition), and the employed reaction mechanism. However, under certain conditions, e.g., small fine structure shares, both reactor types can give comparable results.

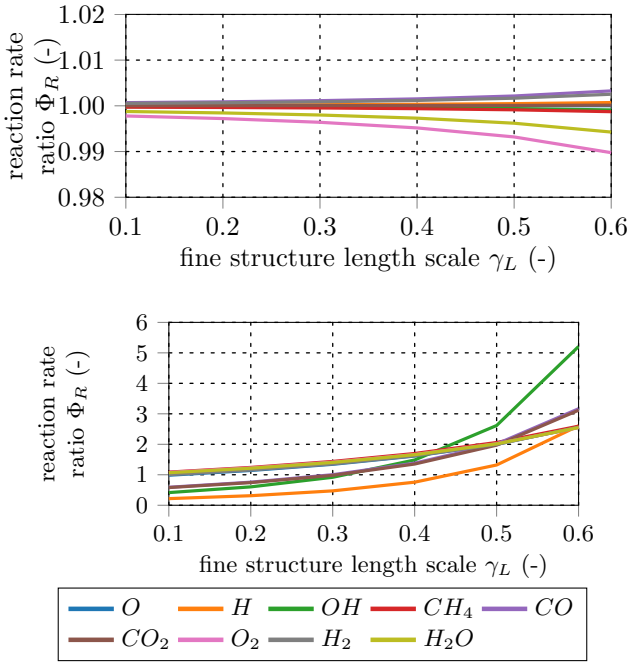

Figure 6. Comparison of the normalized PSR and PFR mean reaction rates for selected main species test cases. (**Top**): temperature 2000 K, stoichiometric mixture, fine structure residence time 1 s, (**Bottom**): temperature 1000 K, lean mixture, fine structure residence time 10^{-3} s.

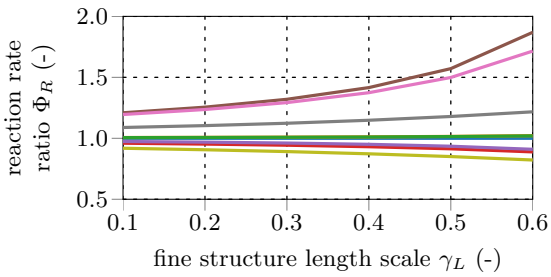

Figure 7. *Cont.*

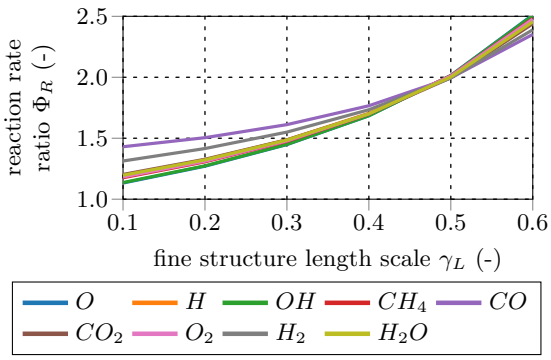

Figure 7. Comparison of the normalized PSR and PFR mean reaction rates for selected radical species test cases. (**Top**): Temperature 2200 K, fine structure residence time 1 s, (**Bottom**): Temperature 2000 K, fine structure residence time 10^{-7} s.

6. Influences of the Model Variations in Flame Modeling

The influences of the proposed model variations are tested using Sandia Flame D, piloted under a stoichiometric premixed jet flame [22,23] surrounded by an air co-flow. The jet Reynolds number is approx. 22,400 and the visible flame length approx. 0.48 m. Table 3 shows the properties of the three gas streams (methane jet, pilot and co-flow stream), which are used as input parameters for the Flame D simulations.

Table 3. Species mass fractions, temperatures and velocities of the jet, pilot, and co-flow of Sandia Flame D [22,23].

Species $\frac{kg}{kg}$	**Jet**	**Pilot**	**Co-flow**
CH_4	0.156	-	-
CO	-	0.004	-
CO_2	-	0.110	-
H	-	2.5×10^{-5}	-
H_2	-	1.3×10^{-4}	-
H_2O	-	0.094	0.006
N_2	0.648	0.735	0.758
O_2	0.196	0.054	0.236
OH	-	0.003	-
$T_{in}(K)$	294	1880	291
u_{in} $(\frac{m}{s})$	49.6	11.4	0.9

The flame is modeled using OpenFOAM® [24] and in-house libraries for the EDC model. Differential diffusion was neglected, since turbulent diffusion is dominant at high turbulence conditions. Although the modeling results are compared to the measured flame data, the main focus is on identifying the model differences. Therefore, a relatively coarse wedge grid with approx. 6090 cells is used. It has a 0.1 m upstream part for the methane jet and pilot inlet; the downstream part is 0.5 m in length and 0.15 m in radial direction. All five EDC modifications were tested on this grid using the PSR and PFR fine structure treatment, summing up ten test cases for the evaluation of the model differences and the fine structure treatment. The EDC2016 and EDC2017 were included in these tests to verify their validity for classical combustion conditions. Obviously, there should be no differences to the EDC1996, since the EDC2016 and EDC2017 are exactly the same as the EDC1996, if the model constants are limited to their standard values in the high turbulent regions. The chemical time scale

(τ_{chem}) of Ren and Goldin [33] is employed to determine the EDC model constants in the EDC2016 and EDC2017 modification:

$$\tau_{chem} = min\left(\frac{\rho_i}{\overline{R}_i}\right)\Bigg|_{\overline{R}_i<0}. \tag{28}$$

Figure 8 compares the main species (CH_4, O_2, CO_2, and H_2O) mass fractions along the center line. In general, all variations give similar results except for the original EDC employing the PFR fine structure treatment, which did not ignite the mixture. Although no detailed investigation was conducted, the EDC reaction rate conversion factor, which is the lowest of all the EDC versions, might be the reason. Moreover, the other results show reasonable agreement to the experimental data. Due to almost identical results, lines in the subsequent diagrams overlap and only some are visible.

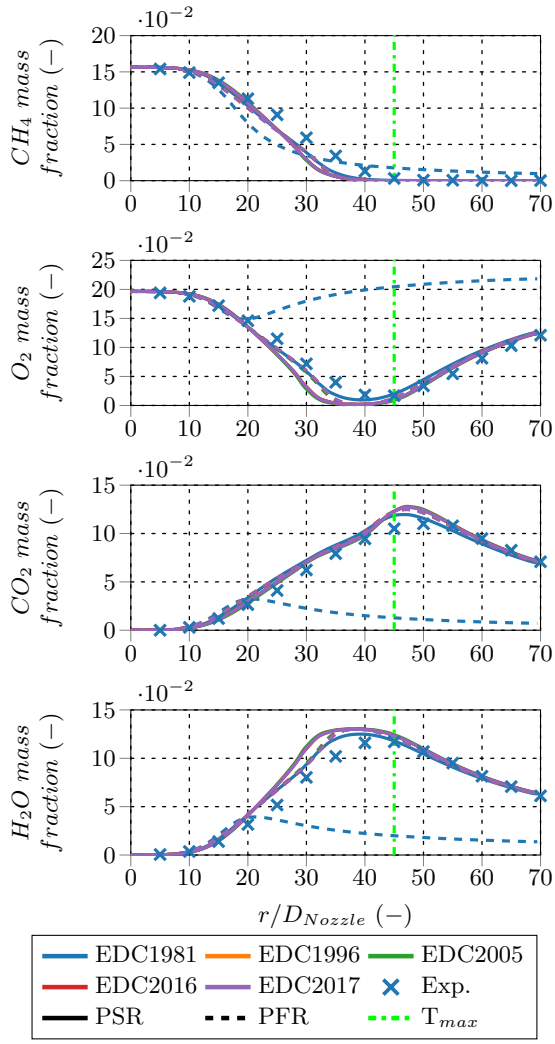

Figure 8. Centerline profiles of main species (CH_4, O_2, CO_2, and H_2O) mass fractions of flame D for all EDC model variations compared to the experimental data from [22]. Not all EDC versions are visible due to overlapping profiles.

Figure 9 shows the species mass fraction profiles of intermediate species (CO, H_2, and OH) as well as the temperature profile along the center line. Compared to the main species, results for intermediates deviate more among the EDC modifications. However, only the OH radical profiles show distinct differences between the PSR and PFR fine structure treatment. The PFR OH peak mass fraction is approx. 1.5 times the PSR peak mass fraction, while the peak position and the profile shapes are similar. In this region, the PSR treatment is closer to the measured values. Temperature profiles confirm that

the EDC1981 employing the PFR fine structure treatment failed to ignite the methane jet; therefore, this variant is excluded from further investigations. The other profiles resemble each other and show reasonable agreement with the measured temperatures.

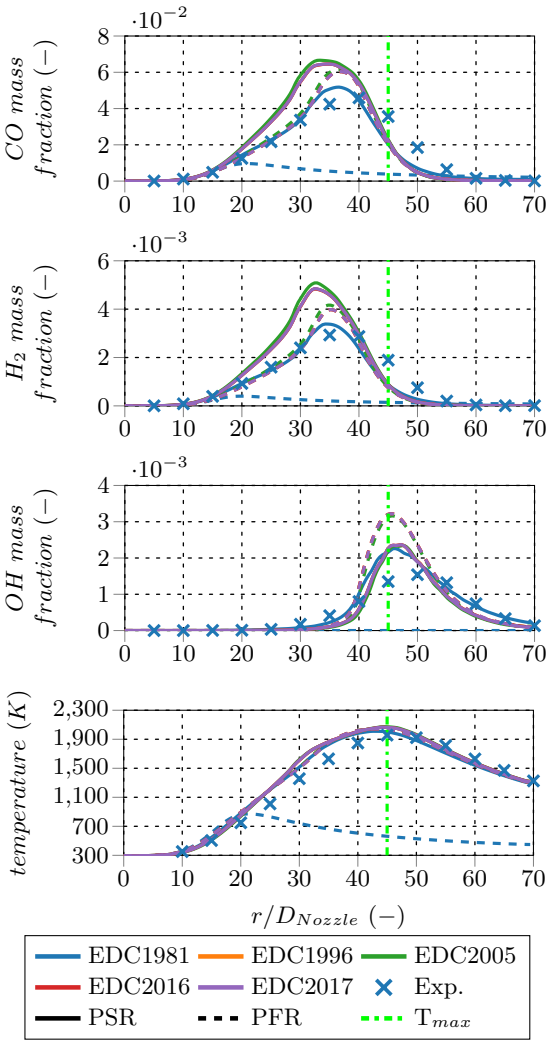

Figure 9. Centerline profiles of intermediate species (CO, H_2, and OH) mass fractions and temperature (T) of flame D for all EDC model variations compared to the experimental data from [22]. Not all EDC versions are visible due to overlapping profiles.

For a better quantification of the fine structure treatment influence, the PFR results are normalized using the PSR results of the corresponding EDC modification. In contrast to the species mass fraction profiles, these normalized profiles reveal more pronounced deviations between the PSR and PFR treatment. Especially for low species mass fractions, the PFR approach predicts up to several times higher or lower concentrations for consumed and produced species, respectively. Methane (CH_4) and oxygen (O_2) deviate the most 20 x/D upstream from the peak temperature, which is located at $x/D \sim 45$. The PFR first predicts higher mass fractions than the PSR followed by lower ones (see Figure 10).

Carbon dioxide (CO_2) and water vapor (H_2O) mass fractions are higher for the PFR downstream from the burner nozzle, but similar further downstream from the PSR values. In contrast, CO and H_2 mass fractions are higher for the PSR approach upstream from the peak temperature, while PFR and PSR results are similar further downstream (see Figure 11). OH radical mass fractions are significantly overpredicted by the PFR treatment compared to the PSR treatment directly above the burner tip

(located at $x/D = 0$) and around the peak temperature location. Both give similar mass fractions further downstream, while OH mass fractions are higher for the PSR upstream. The deviations of the different profiles in the inlet and outlet regions of the intermediate species and CH_4 profiles are caused by numerical fluctuations for these amounts which are close to zero. The normalized temperature profile reveals that the PFR approach predicts slightly higher temperatures downstream from the burner tip. Starting at $x/D \sim 25$, the PSR treatment predicts higher temperatures, but they converge further downstream. The maximum temperature deviation between the two fine structure treatments is around 10%.

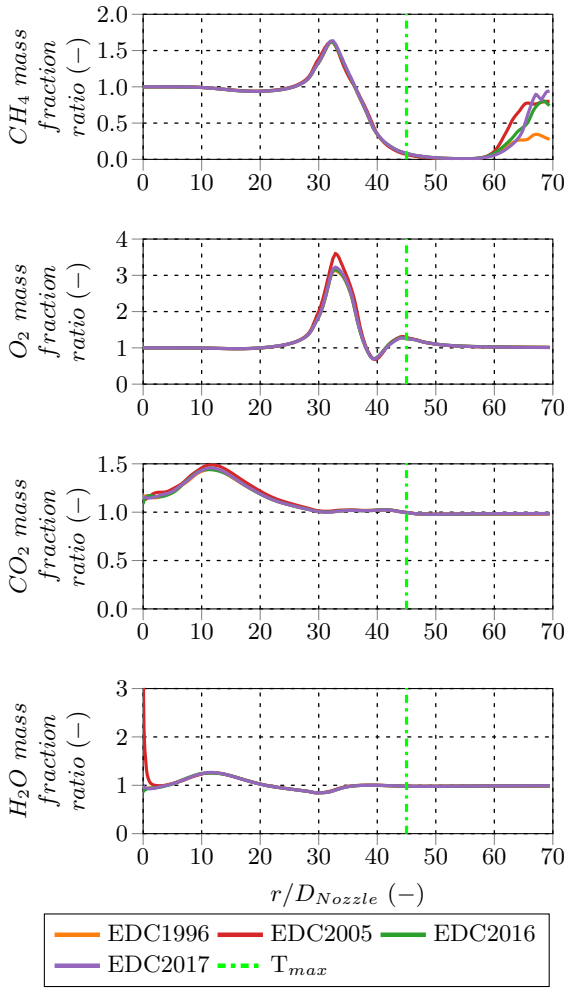

Figure 10. Ratios of PFR versus PSR centerline profiles of main species (CH_4, O_2, CO_2, and H_2O) mass fractions of flame D for all EDC model variations. Not all EDC versions are visible due to overlapping profiles.

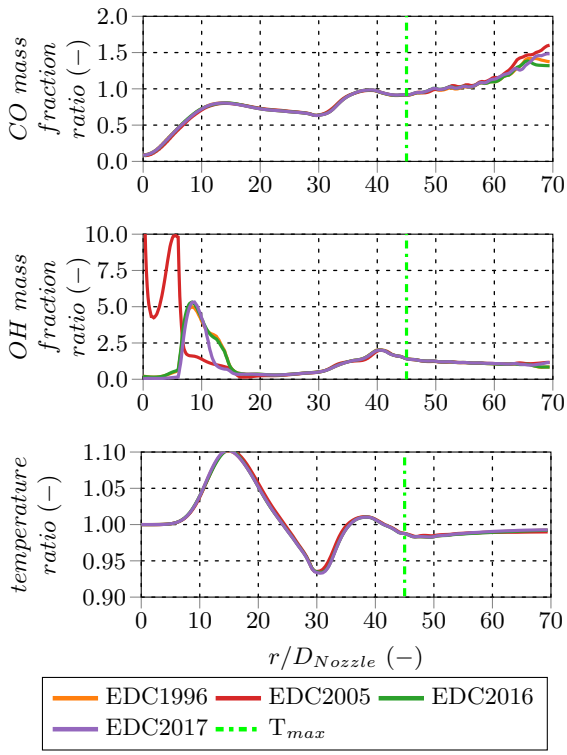

Figure 11. Ratios of PFR versus PSR centerline profiles of intermediate species (CO, H_2, and OH) mass fractions and temperatures (T) of flame D for all EDC model variations. Not all EDC versions are visible due to overlapping profiles.

Comparing the fine structure share (γ^*) and the fine structure residence time (τ^*) along the centerline reveals that the values of the PFR and PSR treatment differ in the range between $x/D \sim 5$ and $x/D \sim 45$ for all EDC modifications (see Figure 12). Up to $x/D \sim 35$, the fine structure share of the PFR computations is lower than using the PSR treatment. Further downstream, both fine fraction treatments predict similar fine structure shares. Assessing the species and relative species mass fraction profiles in this context shows that their deviations correlate with the variations in the fine structure shares (γ^*). Moreover, the EDC2005 fine structure shares are considerably higher than the ones of the other model variations, e.g., EDC1981 and EDC1996, which are virtually similar. That is obvious, since the fine structure share definition differs, e.g., Equation (10) for EDC2005 and Equation (3) for the other EDC versions. The EDC2016 and EDC2017 modifications give identical results as the EDC1996, thus the EDC1996 and EDC2016 values are overlapping in Figure 12. The fine structure deviations appear at the axial positions between $x/D \sim 5$ and $x/D \sim 45$, while the residence times deviate all over the investigated profile. Along the centerline, the normalized fine structure shares and residence times are identical for all EDC modifications, except the EDC2005 fine structure share, which deviates per definition. The fine structure residence times are similar for all investigated cases, although the cases employing the PFR treatment predict higher fine structure residence times than the PSR around $x/D \sim 40$. The original EDC employing the PFR treatment (which failed to ignite the mixture) gives different residence times: lower ones up to $x/D \sim 55$ and higher ones further downstream.

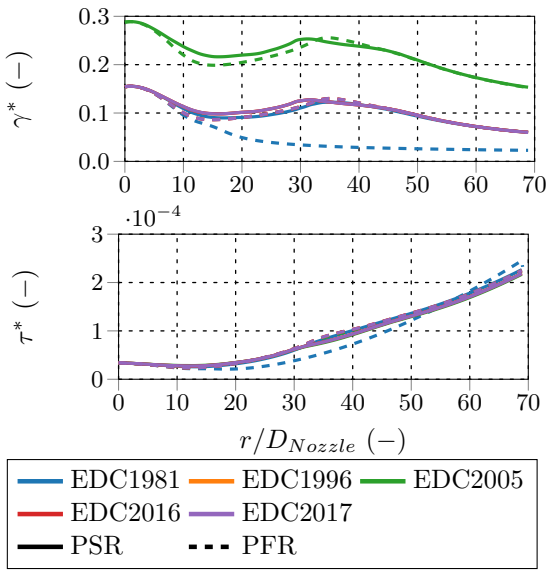

Figure 12. Fine structure share (γ^*) and fine structure residence time (τ^*) along the center axis of flame D for all EDC model variations. Not all EDC versions are visible due to overlapping profiles.

For a better understanding of the variations in the PSR and PFR treatment, the species reaction rates along the center axis were investigated. Figure 13 shows the main species (e.g., CH_4, O_2, CO_2, and H_2O) rates for all EDC variations. The fluctuating rate profiles of the PSR treatment are probably caused by periodic oscillating states or numerical effects occurring when solving the PSR to steady-state. In contrast, the PFR rate profiles are smooth. The CH_4, O_2, and H_2O consumption peaks of the PSR treatment are shifted approx. 5 x/D upstream compared to the PFR peaks. Moreover, the PSR peak magnitudes are almost twice as high as the PFR peak magnitudes. In contrast to the other main species rates, CO_2 is both produced and consumed along the flame D centerline. An initial production at $x/D \sim 30$ is followed by a consumption zone and a second production zone between $x/D \sim 35$ and 40 and $x/D > 40$, respectively. The predicted consumption peak and the second production peak are similar in position and magnitude for both the PSR and PFR fine structure treatment. The rates of the EDC1981 employing the PFR fine structure treatment shows species rates around zero, since the model failed to ignite the mixture.

The species consumption rate profiles of the intermediate species are given in Figure 14. The PSR fine structure treatment predicts CO and H_2 production peaks approx. 5 x/D upstream from the PFR rates. Peak magnitudes are about the same for CO and higher for H_2 in case of the PSR treatment. Starting at $x/D \sim 40$, CO and H_2 are consumed at almost similar rates for both fine structure treatments. In case of OH, the PFR fine structure treatment predicts a consumption peak shortly upstream that of the PSR treatment and has twice the magnitude. The PFR treatment gives smooth profiles, which shows an area of OH production between $x/D \sim 40$ and 45 and a second consumption zone further downstream. After the initial production peak, the rates predicted by PSR treatment are alternating between consumption and production up to $x/D \sim 50$, eventually reaching consumption far downstream. In general, the species consumption rates predicted by the PSR fine structure treatment indicate an earlier combustion start and higher rates than the PFR treatment. Furthermore, the CO, CO_2 and OH rate profiles project the inner and outer reaction zone occurring in Sandia Flame D. The PFR profiles are smooth, while the PSR ones are volatile in this investigation. The PSR behavior is likely caused by oscillating internal states during the solution procedure of the fine structures due to effects caused by the reaction system.

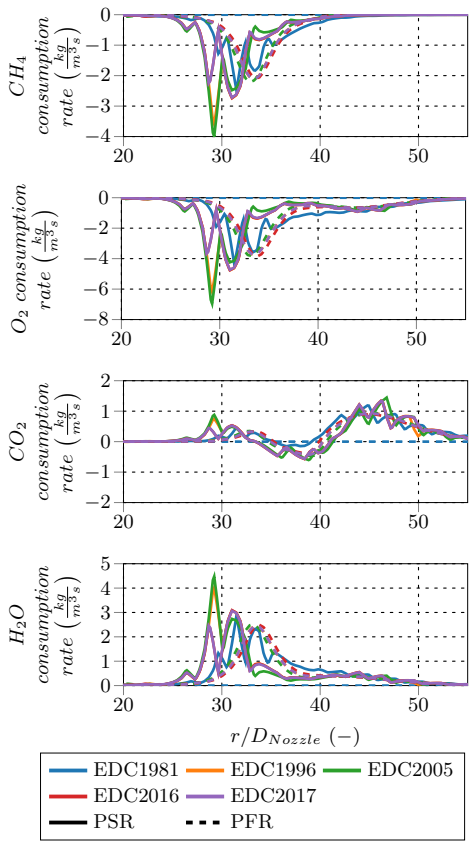

Figure 13. Centerline profiles of main species (CH_4, O_2, CO_2, and H_2) production or consumption rates of flame D for all EDC model variations. Not all EDC versions are visible due to overlapping profiles.

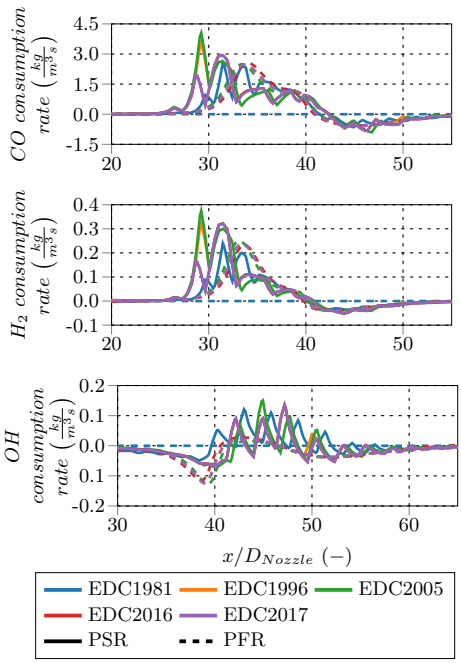

Figure 14. Centerline profiles of intermediate species (CO, H_2, and OH) production or consumption rates of flame D for all EDC model variations.

7. Conclusions

The focus of the present work is the comparison of the classical formulation of the Eddy Dissipation Concept (EDC) and its proposed modifications and variations in literature. A special focus is to extend the knowledge on the consequences of the plug flow reactor (PFR) simplification compared to the perfectly stirred reactor (PSR) fine structure treatment required by the EDC. Only schematic investigations of the PSR vs. PFR approach have been published in literature so far [16–18]. Thus, for the first time, a thorough evaluation of the consequences of the PFR approach is presented. The investigations are based on simple tests and a Sandia Flame D modeling [22,23] study. On top, the proposed EDC improvements [3–8] are discussed in detail and their influence on the EDC results is also evaluated. The findings of the present study are summarized in the following points:

- The fine structures are treated as perfectly stirred (PSR) or plug flow (PFR) reactors in literature [4,6,16,17], although only the PSR treatment complies with the original EDC theory. A simple test series employing a single fluid element is used to study the fine structure treatment influence on the reaction rates. The results indicate increasing deviations between the PSR and PFR approaches for increasing fine structure shares (γ^*) and decreasing fine structure residence times (τ^*).
- Sandia Flame D [22,23] was modeled with an EDC extension for OpenFOAM® [24] to identify the influences of EDC variations with special focus on PSR and PFR fine structure treatment. The thorough investigation of the simulation results along the flame D center axis reveals that there is a difference between the PSR and PFR fine structure treatment for classical combustion conditions, e.g., high turbulence and fast chemistry (mixing controlled). The difference strongly depends on the local EDC parameters γ^* and τ^* as well as the characteristic chemical time scale. Nevertheless, taking into account the coarse grid, all investigated EDC variations (e.g., fine structure treatment, EDC formulation) give reasonable results. In general, the PFR treatment gives better results for CO and H_2 mass fraction profiles, while the PSR treatment gives better results for the OH mass fractions. The species mass fraction ratios reveal deviations between the PSR and PFR approach of more than 50% for the main and intermediate species, while temperatures deviate by up to 10%. Comparing the species consumption rates indicates an earlier combustion start and higher peak reaction rates for the PSR treatment. Both the fine structure share (γ^*) and the fine structure residence time (τ^*) vary up to 15%. Additionally, the consumption rate peaks are generally higher for the PSR approach. The original EDC employing the PFR approach failed to ignite Sandia Flame D in the simulation; the reasons were not investigated in detail.

The results indicate that the PFR fine structure treatment can give reasonable results for classical combustion conditions. Due to its significantly lower numerical effort compared to the PSR fine structure treatment, the PFR approach might be preferred for a priori investigations. However, a thorough selection should be done before choosing the fine structure treatment, if emphasis is put on detailed information of the reaction zone, e.g., intermediate species profiles.

Author Contributions: Conceptualization, M.B., E.-M.W., C.J. and M.H.; Methodology, M.B. and C.J.; Software, M.B. and E.-M.W.; Validation, M.B. and E.-M.W.; Formal Analysis, M.B.; Investigation, M.B.; Resources, M.B., E.-M.W.; Writing—Original Draft Preparation, M.B.; Writing—Review and Editing, M.B., E.-M.W., C.J., and M.H.; Visualization, M.B.; Supervision, C.J. and M.H.; Project Administration, M.H.; Funding Acquisition, M.H.

Funding: The authors gratefully acknowledge the funding support of K1-MET GmbH (Linz, Austria), metallurgical competence center. The research program of the competence center K1-MET is supported by COMET (Competence Center for Excellent Technologies), the Austrian program for competence centers. COMET is funded by the Federal Ministry for Transport, Innovation and Technology, the Federal Ministry for Science, Research and Economy, the province of Upper Austria, Tyrol, and Styria, the Styrian Business Promotion Agency.

Acknowledgments: The computational results presented have been achieved in part using the Vienna Scientific Cluster (VSC). The authors acknowledge the TU Wien University Library for financial support through its Open Access Funding Programme. The authors appreciate the valuable and profound comments of Dr. Bernhard König of the K1-MET GmbH.

Conflicts of Interest: The authors declare no conflict of interest.

References

1. Magnussen, B.F.; Hjertager, B.H. On mathematical modeling of turbulent combustion with special emphasis on soot formation and combustion. *Symp. Int. Combust.* **1977**, *16*, 719–729. [CrossRef]
2. Magnussen, B.F.; Hjertager, M.B.H.; Olsen, J.G.; Bhaduri, D. Effects of turbulent structure and local concentrations on soot formation and combustion in C2H2 diffusion flames. *Symp. Int. Combust.* **1979**, *17*, 1383–1393. [CrossRef]
3. Magnussen, B.F. On the structure of turbulence and a generalized Eddy Dissipation Concept for chemical reaction in turbulent flow. In Proceedings of the 19th Aerospace Sciences Meeting, St. Louis, MO, USA, 12–15 January 1981. [CrossRef]
4. Magnussen, B.F. Modeling of NO_X and Soot Formation by the Eddy Dissipation Concept. *Int. Flame Res. Found.* **1989**, *1989*, 17–19.
5. Gran, I.R.; Magnussen, B.F. A Numerical Study of a Bluff-Body Stabilized Diffusion Flame. Part 2. Influence of Combustion Modeling And Finite-Rate Chemistry. *Combust. Sci. Technol.* **1996**, *119*, 191–217. [CrossRef]
6. Magnussen, B.F. The Eddy Dissipation Concept—A Bridge Between Science and Technology. In Proceedings of the ECCOMAS Thematic Conference on Computational Combustion, Lisbon, Portugal, 21–24 June 2005.
7. Parente, A.; Malik, M.R.; Contino, F.; Cuoci, A.; Dally, B.B. Extension of the Eddy Dissipation Concept for turbulence/chemistry interactions to MILD combustion. *Fuel* **2016**, *163*, 98–111. [CrossRef]
8. Bao, H. Development and Validation of a New Eddy Dissipation Concept (EDC) Model for MILD Combustion. Master's Thesis, Delft University of Technology, Delft, The Netherlands, 2017.
9. Evans, M.J.; Medwell, P.R.; Tian, Z.F. Modeling Lifted Jet Flames in a Heated Coflow Using an Optimized Eddy Dissipation Concept Model. *Combust. Sci. Technol.* **2015**, *187*, 1093–1109. [CrossRef]
10. Weber, R.; Smart, J.P.; vd Kamp, W. On the MILD combustion of gaseous, liquid, and solid fuels in high temperature preheated air. *Proc. Combust. Inst.* **2005**, *30*, 2623–2629. [CrossRef]
11. Cavaliere, A.; de Joannon, M. MILD combustion. *Prog. Energy Combust. Sci.* **2004**, *30*, 329–366. [CrossRef]
12. Poinsot, T.; Veynante, D. *Theoretical and Numerical Combustion*, 2nd ed.; R.T. Edwards, Inc.: Philadelphia, PA, USA, 2005.
13. Mastorakos, E.; Cant, R.S. *An Introduction to Turbulent Reacting Flows*; Imperial College Press: London, UK, 2008.
14. Kuo, A.Y.S.; Corrsin, S. Experiments on internal intermittency and fine-structure distribution functions in fully turbulent fluid. *J. Fluid Mech.* **1971**, *50*, 285–319. [CrossRef]
15. Kuo, A.Y.S.; Corrsin, S. Experiment on the geometry of the fine-structure regions in fully turbulent fluid. *J. Fluid Mech.* **1972**, *56*, 447–479. [CrossRef]
16. Li, Z.; Cuoci, A.; Sadiki, A.; Parente, A. Comprehensive numerical study of the Adelaide Jet in Hot-Coflow burner by means of RANS and detailed chemistry. *Energy* **2017**, *139*, 555–570. [CrossRef]
17. De, A.; Oldenhof, E.; Sathiah, P.; Roekaerts, D. Numerical simulation of Delft-Jet-in-Hot-Coflow (DJHC) flames using the Eddy Dissipation Concept model for turbulence–chemistry interaction. *Flow Turbul. Combust.* **2011**, *87*, 537–567. [CrossRef]
18. Lewandowski, M.T.; Ertesvåg, I.S. Analysis of the Eddy Dissipation Concept formulation for MILD combustion modelling. *Fuel* **2018**, *224*, 687–700. [CrossRef]
19. Minotti, A.; Sciubba, E. LES of a Meso Combustion Chamber with a Detailed Chemistry Model: Comparison between the Flamelet and EDC Models. *Energies* **2010**, *3*, 1943–1959. [CrossRef]
20. Farokhi, M.; Birouk, M. Application of Eddy Dissipation Concept for Modeling Biomass Combustion, Part 2: Gas-Phase Combustion Modeling of a Small-Scale Fixed Bed Furnace. *Energy Fuels* **2016**, *30*, 10800–10808. [CrossRef]
21. Farokhi, M.; Birouk, M. Application of Eddy Dissipation Concept for Modeling Biomass Combustion, Part 1: Assessment of the Model Coefficients. *Energy Fuels* **2016**, *30*, 10789–10799. [CrossRef]

22. Barlow, R.S.; Karpetis, A.N.; Frank, J.H.; Chen, J.Y. Scalar profiles and NO formation in laminar opposed-flow partially premixed methane/air flames. *Combust. Flame* **2001**, *127*, 2102–2118. [CrossRef]
23. Schneider, C.; Dreizler, A.; Janicka, J.; Hassel, E.P. Flow field measurements of stable and locally extinguishing hydrocarbon-fuelled jet flames. *Combust. Flame* **2003**, *135*, 185–190. [CrossRef]
24. Weller, H.G.; Tabor, G.; Jasak, H.; Fureby, C. A tensorial approach to computational continuum mechanics using object-oriented techniques. *Comput. Phys.* **1998**, *12*, 620–631. [CrossRef]
25. Ertesvåg, I.S.; Magnussen, B.F. The Eddy Dissipation Turbulence Energy Cascade Model. *Combust. Sci. Technol.* **2007**, *159*, 213–235. [CrossRef]
26. Lewandowski, M.T.; Ertesvåg, I.S. The impact of the fine structure reactor formulation in the Eddy Dissipation Concept for MILD combustion modelling. In Proceedings of the 11th ERCOFTAC Engineering, Turbulence, Modelling and Measurement, Palermo, Italy, 21–23 September 2016.
27. Lewandowski, M.T.; Ertesvåg, I.S.; Pozorski, J. Influence of the Reactivity of the Fine Structures in Modelling of the Jet-In-Hot-Coflow Flames with the Eddy Dissipation Concept. In Proceedings of the 8th European Combustion Meeting, Dubrovnik, Croatia, 18–21 April 2017.
28. Shiehnejadhesar, A.; Mehrabian, R.; Scharler, R.; Goldin, G.M.; Obernberger, I. Development of a gas phase combustion model suitable for low and high turbulence conditions. *Fuel* **2014**, *126*, 177–187. [CrossRef]
29. Ó Conaire, M.; Curran, H.J.; Simmie, J.M.; Pitz, W.J.; Westbrook, C.K. A comprehensive modeling study of hydrogen oxidation. *Int. J. Chem. Kinet.* **2004**, *36*, 603–622. [CrossRef]
30. Goodwin, D.G.; Moffat, H.K.; Speth, R.L. Cantera: An Object-Oriented Software Toolkit for Chemical Kinetics, Thermodynamics, and Transport Processes. Version 2.3.0, 2017. Available online: http://www.cantera.org (accessed on 11 June 2018).
31. Tennekes, H. Simple Model for the Small-Scale Structure of Turbulence. *Phys. Fluids* **1968**, *11*, 669–671, doi:10.1063/1.1691966. [CrossRef]
32. Smith, G.P.; Golden, D.M.; Frenklach, M.; Moriarty, N.W.; Eiteneer, B.; Goldenberg, M.; Bowman, C.T.; Hanson, R.K.; Song, S.; Gardiner, W.C., Jr.; et al. GRI-Mech 3.0.2018. Available online: http://www.me.berkeley.edu/gri_mech/ (accessed on 11 June 2018).
33. Ren, Z.; Goldin, G.M. An efficient time scale model with tabulation of chemical equilibrium. *Combust. Flame* **2011**, *158*, 1977–1979. [CrossRef]

© 2018 by the authors. Licensee MDPI, Basel, Switzerland. This article is an open access article distributed under the terms and conditions of the Creative Commons Attribution (CC BY) license (http://creativecommons.org/licenses/by/4.0/).